Hindawi
Advances in Civil Engineering
Volume 2024, Article ID 4904489, 20 pages
https://doi.org/10.1155/2024/4904489

Research Article

Influence of Plate Position on Uplift Failure State and Bearing Capacity of NT-CEP Pile Groups

Yongmei Qian,[1] **Xu Chen**,[1] **Lin Sun**,[1] **Xihui Wang**,[2] **and Yang Chen**[1]

[1]*Jilin Jianzhu University, Changchun 130118, China*
[2]*SINOMACH Academy of Science and Technology Co. Ltd., Beijing 100083, China*

Correspondence should be addressed to Yongmei Qian; 654675316@qq.com

Received 13 December 2023; Revised 16 February 2024; Accepted 19 February 2024; Published 1 March 2024

Academic Editor: Paolo Castaldo

The previous research results of the research group demonstrated that the plate position is the main factor affecting the uplift bearing capacity of the new type of concrete expanded plate pile (NT-CEP pile) group and the failure state of the soil around the pile. In this study, the visual half-section pile small-scale model of undisturbed soil tension test and ANSYS Finite Element Software comparative analysis two-pile small-scale test model and two-, four-, six-, and nine-pile models, which included the corner, side, and middle piles, were developed. The effect of the plate position on the displacement, stress, and bearing mechanism of the NT-CEP pile group under vertical tension was determined, which further improved the design concept of the NT-CEP pile group and provided strong theoretical support for its widespread application.

1. Introduction

The new type of concrete expanded plate pile (NT-CEP pile) is an example of a variable cross-sectional pile [1–3]. The addition of a bearing plate improves the bearing capacity and reduces settlement and material costs. During the construction process, mud discharge is reduced by drilling and expanding the pile-forming machine [2, 4, 5], as shown in Figure 1. The uplift bearing capacity of the traditional straight hole pile is mainly provided by the side friction of the pile, while the uplift bearing capacity of the NT-CEP pile is composed of two parts: (1) the side friction of the pile and (2) the end bearing capacity provided by the bearing expansion plate. The uplift bearing capacity provided by the end bearing force is much greater than that provided by the side friction of the pile, so the uplift bearing capacity of the NT-CEP pile is greatly improved compared with traditional straight hole piles. In large-scale bridge engineering and super high-rise buildings sensitive to wind load, because of its high requirements for the uplift bearing capacity of the foundation, the NT-CEP pile also provides a broad space for large-scale application. Recently, theoretical and experimental investigations have been conducted on a single, leading to comprehensive research results [6, 7]. However, little research has been done on NT-CEP pile groups by engineering practices [8–12]. In this study, the bearing capacity of the NT-CEP pile group and the failure state of the soil around the pile were studied theoretically. In particular, the key factor of bearing plate position and the effect of different plate positions on the uplift resistance of a pile group were discussed.

In this study, a new type of real-time observation of NT-CEP double-pile half-section small-scale model undisturbed soil test method and ANSYS finite element software simulation analysis method were used for comparative analysis [13–16]. Two-, four-, six-, and nine-pile models encompassing the corner, side, and middle piles were set up using the test and ANSYS finite element software. Through postprocessing, displacement and stress data were obtained, and the corresponding nephogram and curve analyses were performed [17]. By comparing the effects of different plate positions on the pile body and soil around the NT-CEP pile group under the same working conditions, the influence law of the plate position on the bad state and bearing capacity of the NT-CEP pile group soil is summarized. This lays a solid theoretical foundation for the continuous popularization and application of NT-CEP piles.

Figure 1: Schematic of NT-CEP pile and pile-forming machine.

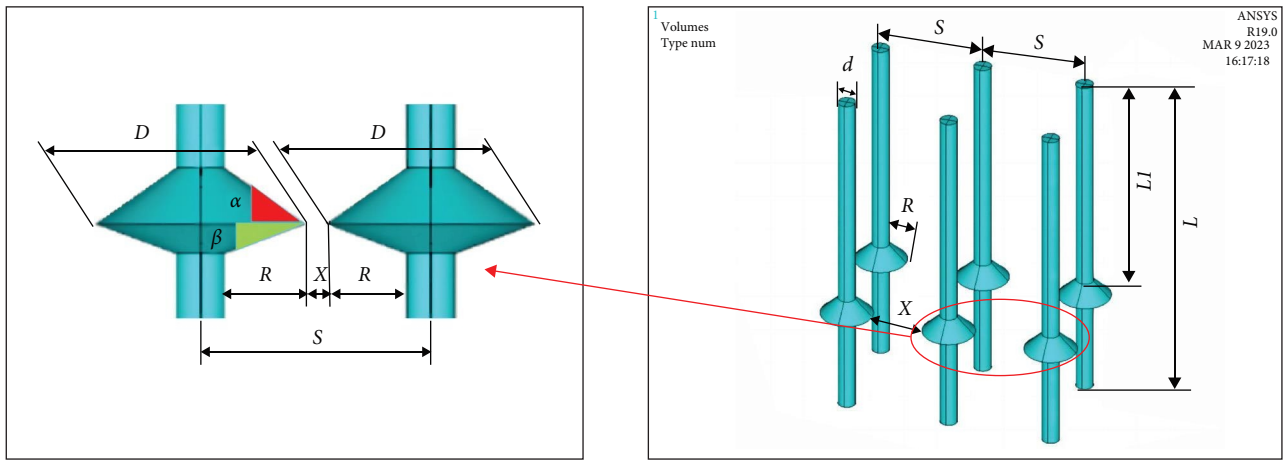

Figure 2: Pile body size and approximate model diagram.

2. Experimental Study on Uplift Resistance of Undisturbed Soil in a Small-Scale Model of Visual Half-Section Pile

In this study, a new half-section NT-CEP double-pile small-scale model undisturbed soil test method developed by our research group was used in the test research part. Compared with the traditional full-section pile research method, this test method has two advantages: (1) The pile–soil interaction and the displacement of soil around the pile could be observed directly in real-time, which could not be achieved by the traditional test method. (2) The small model test was easy to operate and greatly reduced the test cost. Because the main research content of this study was the state change of the failure process of the soil around the pile, the proportional reduction of the specimen size had little effect on the test results. The research group had previously carried out on-site proportional tests, which verified that the proportional reduction test was in good agreement with the actual failure state of the soil around the NT-CEP pile, so the size effect could be ignored. The friction force between the model pile and the observation glass was inevitable, but the purpose of this small-scale test was to qualitatively analyze the failure state of the soil, not to quantitatively analyze the specific tension value, so the friction force between the half-section pile and the observation glass had negligible influence on this test.

2.1. Preparation of Half-Section Model Pile. The half-section pile model used in this study was made by reducing the actual NT-CEP pile according to the ratio of 1 : 40. The aluminum alloy material with stiffness and deformation performance closer to C40 concrete was selected. The pile size is shown in Figure 2. The four groups of model piles made by the specimen processing factory are shown in Figure 3. The pile body size is shown in Table 1.

2.2. Preparation of Undisturbed Soil Samples. The operation steps of soil sampling in the test were as follows:

Cleaning and excavation of the earth borrowing site→-placing the earth borrowing device→ pressing the earth

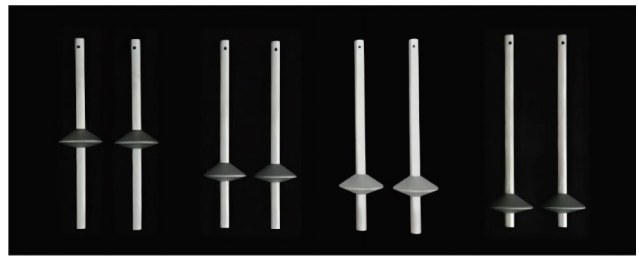

Figure 3: Physical drawings of four groups of model piles.

Table 1: Detailed size table.

Group	$L1$ (mm)	L (mm)	d (mm)	S (mm)	D (mm)	R (mm)	Slope angle of the disk (°)	X (mm)
M1	80 = 4R	200	12.5	80 (4R)	52.5	20	$\alpha = 36°$ $\beta = 21°$	37.5
M2	120 = 6R							
M3	140 = 7R							
M4	160 = 8R							

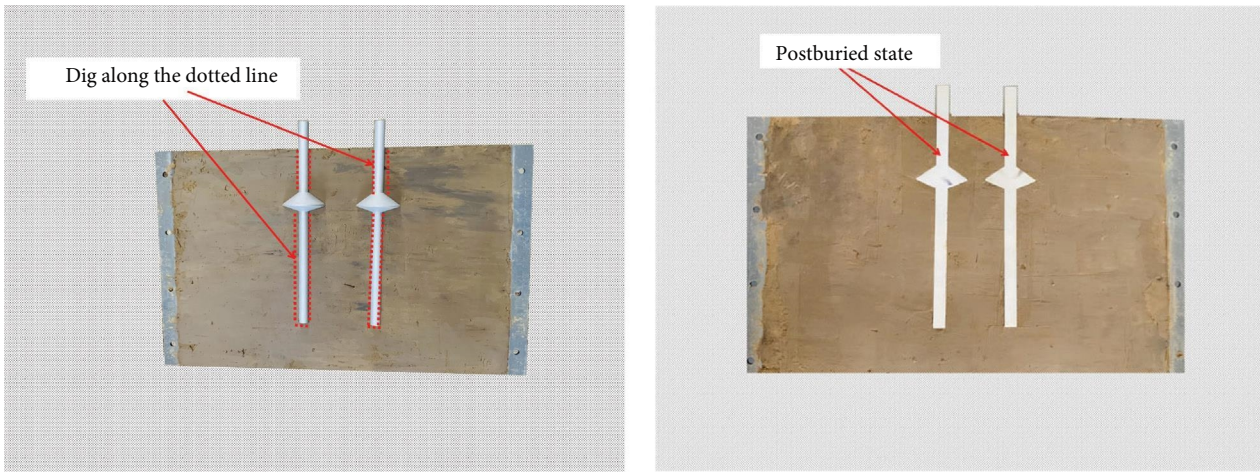

Figure 4: General situation diagram of specimen preparation.

borrowing device into the soil→taking out→dressing the surface clay→ packing with plastic film→transporting it back to the laboratory for storage. The size of the soil sampler was 360 mm × 200 mm × 280 mm. The 5 mm thick steel plate was used to prevent deformation during the soil-taking process. The steel plate could be replaced with tempered glass during the test.

2.3. Preparation of Pile–Soil Specimen. The soil samples sealed and preserved in the laboratory were unpacked, and the double-pile model was buried in the test soil samples. The specific operation steps are as follows: Leveling→ positioning→ marking→trenching→embedding→super leveling. After the pile was buried, the pile–soil specimen was prepared, and the subsequent loading test could be carried out. The general situation of specimen preparation is shown in Figure 4.

2.4. Test Equipment. This test was carried out by a multifunctional test bed independently designed by the research group, as shown in Figure 5(a). To ensure the simultaneous loading of double piles, the research group designed a synchronous loading connector to connect double piles. This connector consisted of a steel plate with long holes, two grooved connecting rods, bolts, and studs. When loaded, the jack was placed between the cross beam and the steel plate of the connector, and the jack jacked up the steel plate of the connector vertically to simulate the vertical upward tension. Because the steel plate of the connector had great rigidity, it could ensure that the tension force distributed by the two connecting rods was the same, as shown in Figure 5(b).

2.5. Test Process. The prepared pile–soil specimens were installed in place on the loading table, and then the loading device was installed for the loading test. The specific steps are as follows: Adjust the placement position of the pile–soil specimen on the loading platform→install pressure plate of pile–soil specimen→ install vertical loading jack and displacement meter→install observation glass→load. The

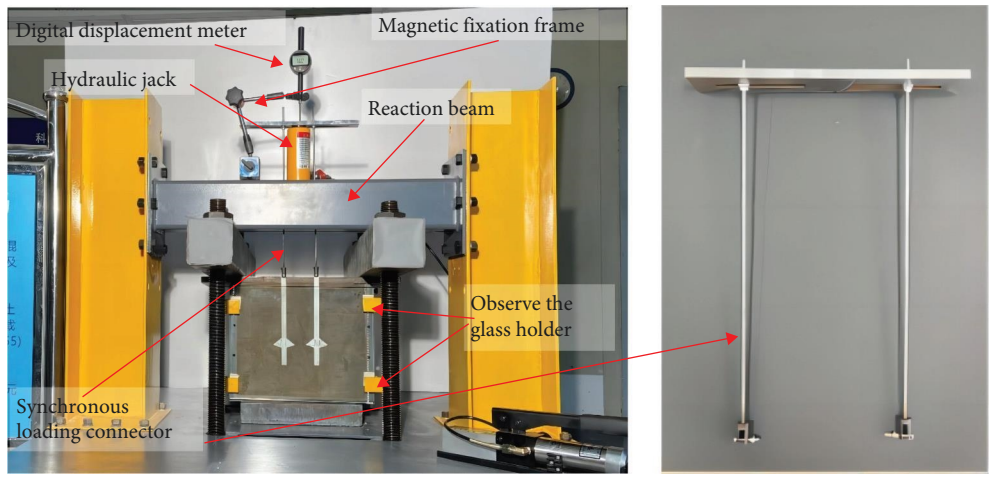

(a) (b)

Figure 5: (a) Multifunctional test bench and (b) synchronous loading connector.

loading process was continuous and uninterrupted, during which the state of the pile and soil was recorded by video recording and regular photographing.

3. Analysis of Pull-Out Test Results of NT-CEP Double Piles

3.1. Analysis of Uplift Failure Process of Double Piles. In this study, the test results of four groups of model piles were analyzed from the aspects of failure process and failure mode, and the load–displacement curves of four groups of model piles were compared and analyzed. The uplift failure process of double-pile specimens in each group of test models was similar. Taking the M2 group as an example, the pull-out failure process is shown in Figure 6.

It could be seen from Figure 6 that when the load was 0–0.7 kN, the top displacement of double piles was very small. When the double piles were loaded to 0.7 kN, the displacement of the top of the pile was 2.53 mm, and the relative displacement of the pile and soil began to occur. The pile and soil on the lower side of the bearing plate were separated, as shown in Figure 6(a). At this time, the double piles mainly relied on side friction to bear the load.

As the load continued to increase, the pressure of the two plates on the upper soil increased continuously. When the pressure of the two plates on the upper soil was greater than the cohesive force between soil particles, horizontal cracks appeared in the soil near the end of the bearing plate of the double piles, and the cracks on the inner side of the two piles appear earlier than the cracks on the outer side, because the compressive stress of the inner soil under the joint action of the two plates was greater than that on the outer side, as shown in Figure 6(b). At the same time, there was a slip area above the load-bearing plate, which shows a watermark in the test, as shown in Figure 6(c), indicating that the soil in this area had slipped and deformed.

With the horizontal cracks at the end of the bearing plate of double piles developing horizontally, when the load reached 0.9 kN, the horizontal cracks penetrated, as shown in Figure 6(d). At this time, the soil at the lower part of the horizontal cracks between double piles completely withdraws from work, and all the soil at the upper part of the plate bears the load from the bearing plate. When the load further increases, the crack width at the end of the double-pile bearing plate gradually increases, as shown in the red circle part of Figure 6(e). The area of soil slip on the upper part of the load-bearing plate also increased, as shown by the green line in Figure 6(e).

When the load increases to 1.5 kN, the shear failure of the soil between the two piles occurs, the width of horizontal cracks no longer increases, and the slip areas of the soil above the bearing plates of the two piles meet, as shown in Figure 6(f).

3.2. Comparative Analysis of Failure State. The final failure state of the undisturbed soil pullout test of four groups of half-section CEP double pile models is shown in Figure 7.

As can be seen from Figure 7, there were two failure states, one of which was the M1 group. When the pile length $L1$ on the plate was small and less than 4R, the soil would be punched after being cracked, as shown in Figure 7(a). The other was that when the pile length $L1$ on the plate was greater than 4R, the soil between the two piles was cracked and the soil on the plate slipped and destroyed, as shown in Figure 7(b)–7(d).

3.3. Load–Displacement Curve Analysis of Undisturbed Soil Pull-Out Test of Double-Pile Model. The load–displacement curves of four groups of double-pile tests are shown in Figure 8.

(1) The load–displacement curves of the four groups of models were almost the same at the initial stage of loading, and the pile top displacement increases linearly with the increase of load. At this time, the load was mainly borne by the friction between the pile and soil, and the plate position had little effect on the bearing capacity of NT-CEP double piles.

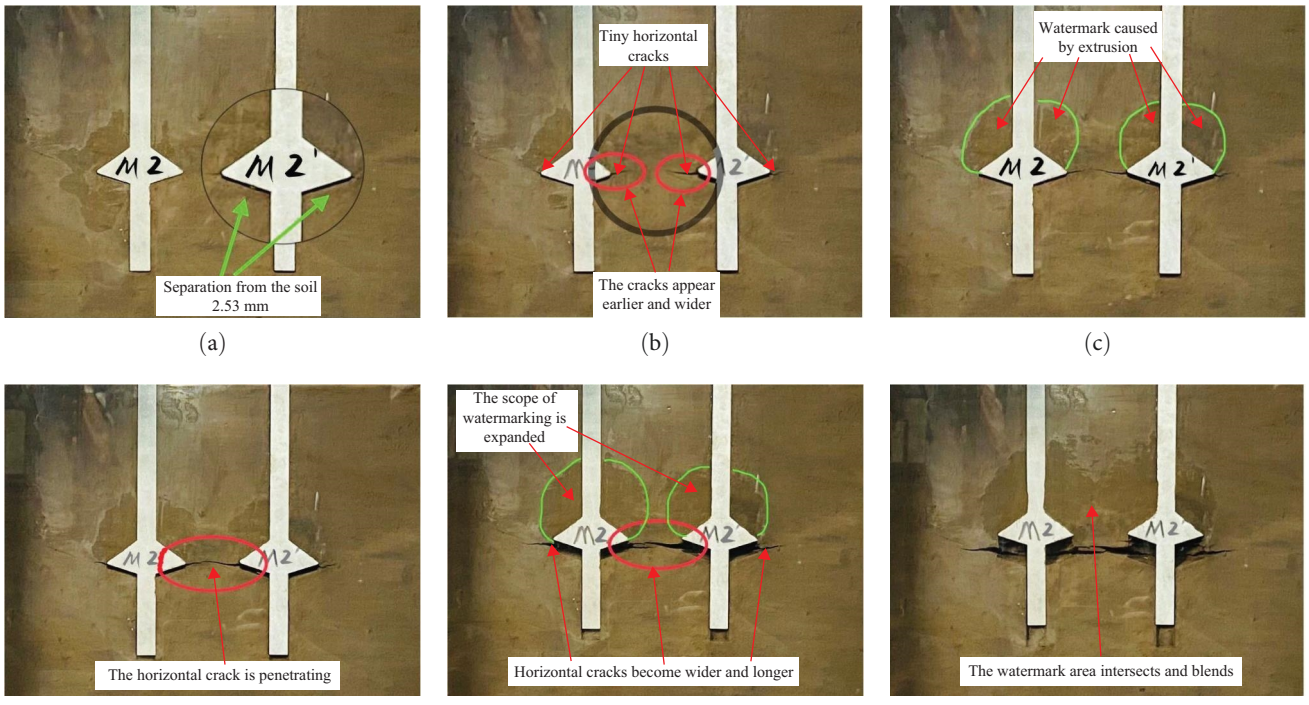

Figure 6: Uplift failure process diagram of M2 group double piles (a)–(f).

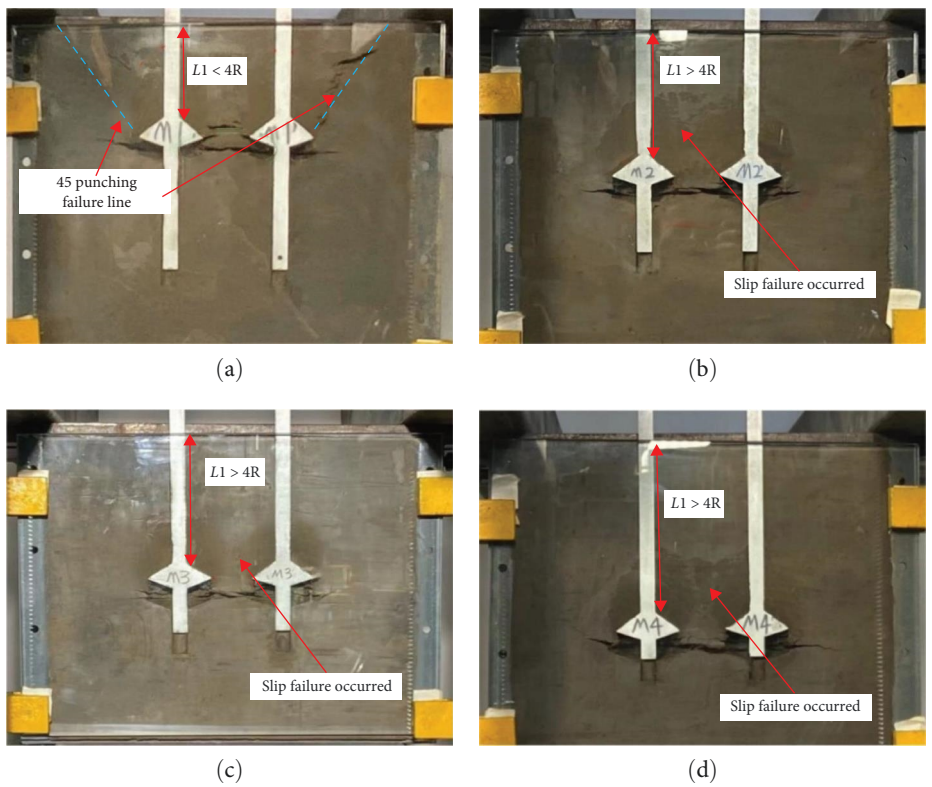

Figure 7: Final failure state of undisturbed soil pullout test of CEP double pile model (a)–(d).

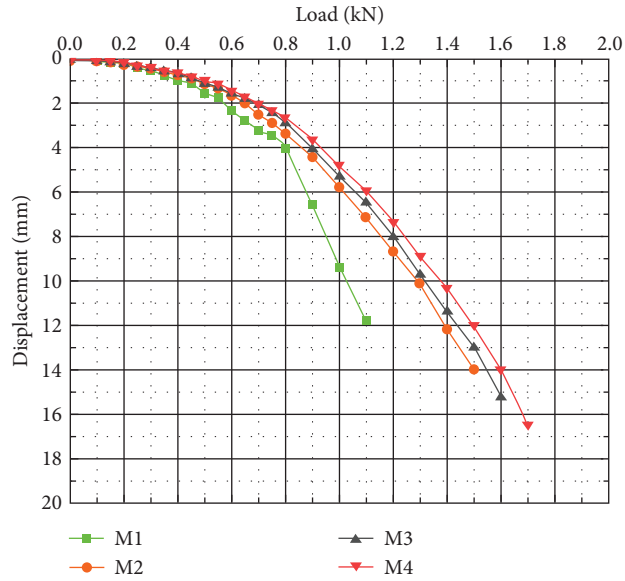

Figure 8: The load–displacement curve of undisturbed soil pull-out test of double-pile model.

Table 2: Pile–soil parameter setting.

Material	Density (t/mm^3)	Elastic modulus (Mpa)	Poisson's ratio	Cohesion (Mpa)	Friction angle (°)	Expansion angle (°)	Pile–soil friction coefficient
Concrete	2.25×10^{-9}	3.465×10^4	0.2	—	—	—	0.3
Clay	1.488×10^{-9}	25	0.35	0.04355	10.7	10.7	

(2) When the load of the M1 model was 0.8 kN, there was an obvious inflection point. Combined with the above test phenomenon, 45 punching inclined cracks began to appear above the load-bearing plate, and the soil was close to punching failure, which was mainly caused by the small pile length $L1$ on the plate.

(3) In the middle and later stages of loading, under the action of the same load, the closer the bearing plate was to the pile end, the smaller the displacement of the pile top and the larger the corresponding load during failure. This was because the load was transmitted to the soil farther away from the bearing plate (the slip zone on the double-pile plate was expanding continuously in the test), and the bearing capacity was not only provided by the small soil on the plate.

4. ANSYS Finite Element Model Construction

4.1. Determination of Constitutive Relation. In practical engineering, an NT-CEP pile is a reinforced concrete structure. In the ANSYS finite element analysis, the reinforced concrete model adopts the integral simulation method to disperse the steel bar in the concrete unit, thereby ignoring the bond-slip between the steel bar and concrete. Because the elastic–plastic model in the elastic–plastic theory can better reflect the stress characteristics of concrete, the concrete constitutive model in this study adopts the elastic–plastic constitutive model [18]. The soil model includes two types: nonlinear elastic and elastic–plastic models. This study adopted the Duncan–Chang model as the nonlinear elastic model.

4.2. Selection of Element Type. For the 3D modeling in this study, the pile body element used was Solid65 [19], which is a reinforced concrete solid element. This has a good simulation effect on the creep and cracking of reinforced concrete in practical engineering applications. The soil element type adopted was Solid45 for the 3D solid elements. The characteristics of this element are consistent with those of cohesive soils used in practical engineering. It can simulate plasticity, stress strengthening, expansion, large deformations, and large strains.

4.3. Selection of Model Material Properties. The material properties of the soil model in this study were determined based on a previous undisturbed soil test conducted by a research group. The NT-CEP pile body refers to a large-scale engineering test in the early stages of research. The material properties of the pile body model were the same as those of C40 concrete. The pile and soil parameters are listed in Table 2.

4.4. Dimensional Parameters of Pile and Soil. In this study, the size of the pile body differed from the previous modeling size of the research group. To approximate the actual project,

Table 3: Data table of different plate positions of two-, four-, six-, and nine-pile models ($R = 800$ mm is the overhang diameter of the plate).

	Groups							
Two-pile	T1	T2	T3	T4	—	—	—	—
Four-pile	—	F1	F2	F3	F4	F5	F6	F7
Six-pile	—	S1	S2	S3	S4	S5	S6	S7
Nine-pile	—	N1	N2	N3	N4	N5	N6	N7
$L1$	4R	6R	7R	8R	9R	10R	12R	14R

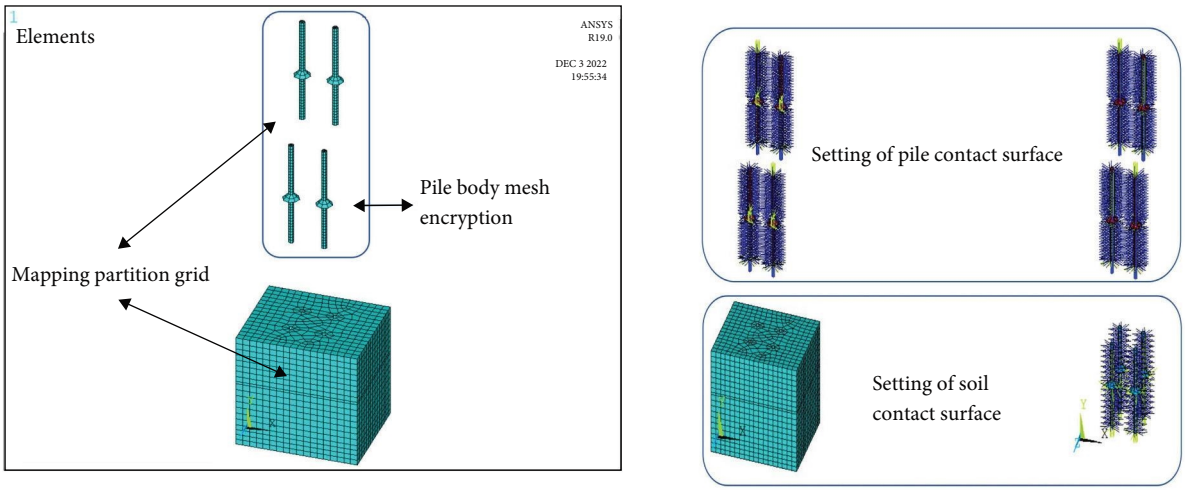

Figure 9: Grid division and contact surface setting effect diagram.

the pile body was constructed as a full section, and the model was created at a scale of 1 : 1 based on real dimensions. After referring to the previous research results of the research group, the reasonable size parameters of pile body and soil were selected and set as follows: pile length $L = 8{,}000$ mm, pile diameter $D = 500$ mm, plate overhang diameter $R = 800$ mm, plate uphill angle $\alpha = 36°$, plate downhill angle $\beta = 21°$, plate diameter $D = 2{,}100$ mm, pile distance $S = 3{,}200$ mm, and clear distance between plates $X = 1{,}500$ mm. These dimensions were designed as invariants. The pile size and approximate model are shown in Figure 2. To remove the influence of boundary conditions on the analysis results, cuboid soil models with lengths, widths, and heights of 11,000, 11,000, and 3,000 mm, respectively, were created. In the design of a single pile, the variable of the plate position (distance $L1$ from the top of the plate to the top of the pile) was investigated, and the $L1$ of each pile in each pile group model is equal.

In this study, four NT-CEP pile group models with two, four, six, and nine piles were considered. Therefore, a corresponding model should be established for the plate position variable. The specific modeling conditions are listed in Table 3. Simultaneously, a set of single-pile models Q1 was established with $L1 = 12$R, and the other parameters were the same as those in the control group.

4.5. Mesh Division and Contact Surface Setting. The mesh partition is the most basic and important link [20]. The mapping partition was chosen in this study because it is suitable for structures with relatively uniform shapes, and its accuracy meets the requirements of this study.

The contact surface between the pile and soil includes a rigid-flexible contact form and a flexible–flexible contact form. In this study, the elastic modulus of the NT-CEP pile model was significantly larger than that of the soil model; therefore, the rigid-flexible contact mode was selected. Target 10 was used for the rigid surface of the pile, contact 173 was used for the flexible surface of the soil, and the friction coefficient between the contact surfaces was set to 0.3. The model obtained after mesh division and contact surface setting is shown in Figure 9.

4.6. Constraint Setting and Load Application. To prevent the irregular displacement of the entire soil from affecting the simulation results during the loading process while considering that the stress of the NT-CEP pile in this study is vertical tension, the degrees of freedom of the top surface in the Y-direction are not constrained, and the rest are constrained in each plane of the hexahedron soil model.

To analyze the changing state of the pile and soil in the entire loading process, the loading of piles was applied step-by-step, and 200 kN of each pile was loaded at each stage. Loading was stopped when the finite element analysis curve did not converge. The model obtained after constraint setting and load application is shown in Figure 10.

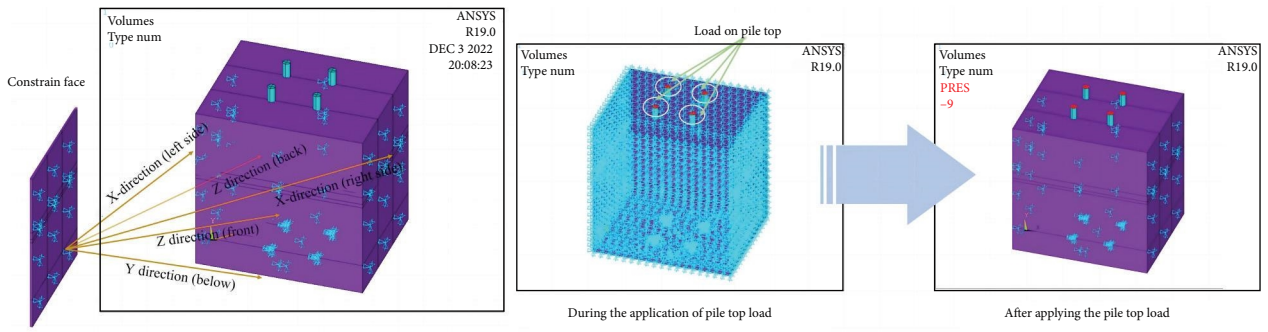

Figure 10: Effect diagram after constraint setting and load application.

5. Analysis of NT-CEP Double Pile ANSYS Finite Element Results

5.1. Analysis of NT-CEP Double Pile ANSYS Displacement Cloud Diagram. The displacement nephogram of the T1 group of several special loading steps was selected to analyze the displacement nephogram of NT-CEP double pile during uplift loading, which was 100, 300, 500, 700, 1,100, and 1,300 kN, respectively, as shown in Figure 11.

As can be seen from the change of displacement nephogram in Figure 11:

(1) When the first stage load was loaded, the uplift load was transmitted to the upper soil of the plate, and the upper soil of the plate was deformed by compression, as shown in Figure 11(a).

(2) When the load was 300−500 kN, as shown in Figures 11(b) and 11(c). The deformation and influence range of the upper part of the two piles increased slowly. The soil between the two plates still participates in the work as a whole and was in the linear working stage.

(3) Figure 11(d), when the load increased to 700 kN, the displacement of the pile top was 25 mm. At this time, the soil between the two pile plates was light green, while the green parts on the two pile plates intersected, which shows that the relative displacement of the soil was penetrated. After 700 kN, due to the aggravation of the relative displacement of the soil between the two pile plates, as shown in Figure 11(e), the soil almost failed. Finally, when the load reached 1,300 kN, the ANSYS simulation analysis no longer converged, the ring was broken, and the loading was terminated.

5.2. NT-CEP Double Pile Load–Displacement Curve Analysis. Analyzing the load–displacement curve of Figure 12 shows that:

(1) The changing trend of the load–displacement curve of each model group at the initial stage of loading was the same; that was, with the increase of load, the vertical displacement of the pile top also increases continuously. The displacement increased linearly with the increase in load. At this time, it mainly depended on friction to resist load.

(2) Under the same load of the T1–T4 group, the bearing capacity of the T1 group was smaller, and it suddenly dropped sharply at 800 kN, and shear failure occurred at this time. T2–T4 groups have a larger uplift bearing capacity, and the T4 group has the largest, so when the pile length $L1$ above the bearing plate was greater than 4R, the lower the bearing plate, the greater the uplift bearing capacity.

6. The Pullout Test of the NT-CEP Double Pile Model Is Compared with ANSYS Simulation Results

6.1. Comparative Analysis of NT-CEP Double Pile Failure Process. The T2 group and M2 group were selected for comparative analysis of the failure process of NT-CEP double piles, and the failure process is shown in Figure 13.

In ANSYS simulation analysis, when loading to about 600 kN, the upper soil was compressed due to the squeezing effect of the double-pile bearing plate on the upper soil, the double piles were displaced upward, and the soil under the double-pile plate was separated from pile and soil, as shown in the yellow circle part in Figure 13(a). In the model test, the phenomenon of pile–soil separation appears when the load reaches 0.7 kN, as indicated by the green arrow in Figure 13(b), and the fitting degree of Figures 13(a) and 13(b) is higher. With the increase of load, the inner cracks of the two piles appear earlier on the outer side, because the inner soil was acted by the two plates together, as shown in the red circle in Figure 13(d), while in ANSYS simulation analysis, this phenomenon was manifested as the displacement difference of the soil, as shown in the enlarged part in Figure 13(c). At the final failure, the slip areas on the two piles of the M2 group meet, as shown by the watermark shape in Figure 13(f) and the yellow area in Figure 13(e). The top of the two piles reaches the maximum displacement.

Through the above comparative analysis, it could be seen that the model test and simulation analysis show good unity in the shape and state of the slip zone on the two piles, the position and width of cracks, and the phenomenon of pile–soil separation under the piles. This not only verifies

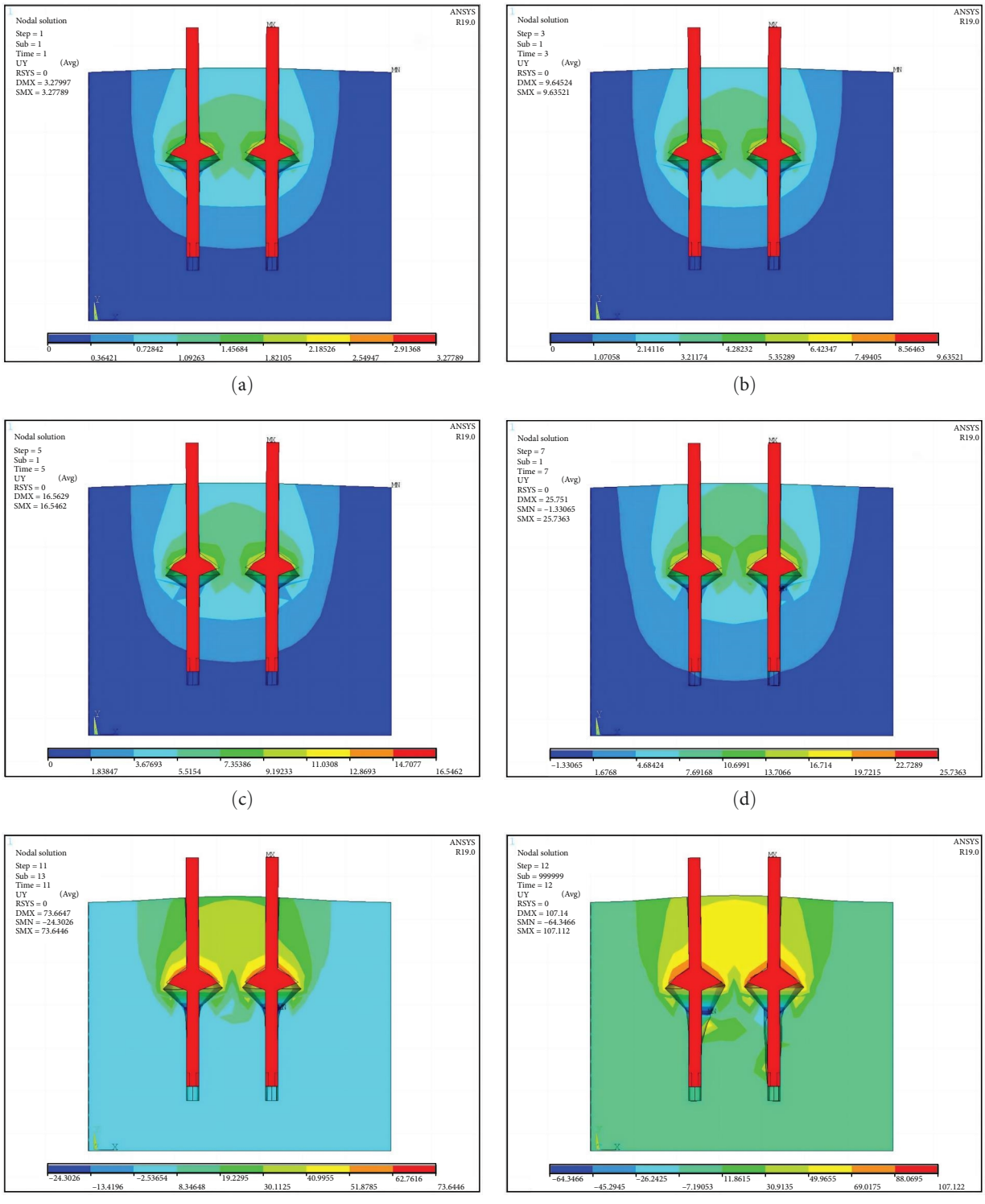

Figure 11: *Y*-direction displacement nephogram of T1 group loading process: (a) 100 kN; (b) 300 kN; (c) 500 kN; (d) 700 kN; (e) 1,100 kN; (f) 1,300 kN.

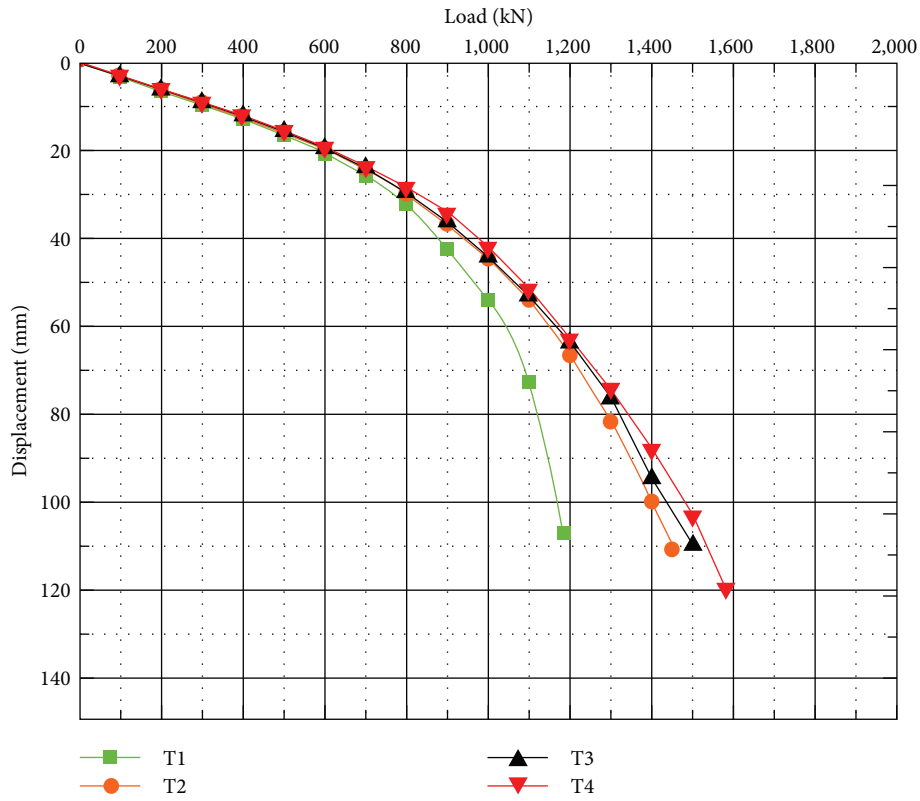

Figure 12: Finite element simulation of the load–displacement curve of double piles.

the validity of the model test results but also proves the scientific nature of the basic assumptions and simulation parameters in the simulation analysis.

6.2. Comparative Analysis of Load–Displacement Curves of NT-CEP Double Piles

(1) No matter the load–displacement curve of the model test or the load–displacement curve in simulation analysis, the curve change trend of four groups of NT-CEP double piles was the same at the initial stage of loading; at this time, NT-CEP double piles mainly provided bearing capacity by measuring friction resistance.

(2) Figures 14 and 15 show obvious inflection points at 0.8 and 800 kN, respectively. Combined with experimental pictures and simulated nephogram phenomenon, it could be seen that 45 punching oblique cracks began to appear obliquely above the load-bearing plate at this time. The state of inflection points in the two figures was roughly the same, which once again confirms the consistency between the NT-CEP double-pile finite element simulation analysis and the half-section model test.

(3) Comparing the curves in Figures 14 and 15, it could be seen that the lower the NT-CEP double pile bearing plate was, the greater its ultimate bearing capacity is.

(4) According to the above analysis, the results of the NT-CEP double pile pull-out model test and simulation analysis were consistent, and they confirmed each other.

7. Analysis of ANSYS Finite Element Simulation Results of Four-, Six-, and Nine-Pile

Because the above comparative analysis verified the validity of the model test results and the scientific nature of the basic assumptions and simulation parameters in the simulation analysis, the four-, six-, and nine-pile were mainly analyzed by finite element simulation.

7.1. Displacement Nephogram Analysis of Four Piles during Loading the Process. To observe the displacement under different loads in detail, the displacement nephograms in the F6 group simulation analysis process were selected. The *Y*-direction displacement nephograms under loads of 1,600, 2,400, 3,200, 4,000, 4,800, 5,600, 6,400, and 7,200 kN were obtained, respectively, as shown in Figure 16.

The following can be observed from the change in displacement nephogram in Figure 16:

(1) At the initial stage of loading, only the pile body had a vertical displacement, and although the soil around the pile was squeezed, the displacement was not evident, as shown in Figures 16(a) and 16(b). At this stage, the NT-CEP pile depends on the side friction of the pile to resist the load; therefore, the displacement change in the pile and the soil around the pile is not obvious.

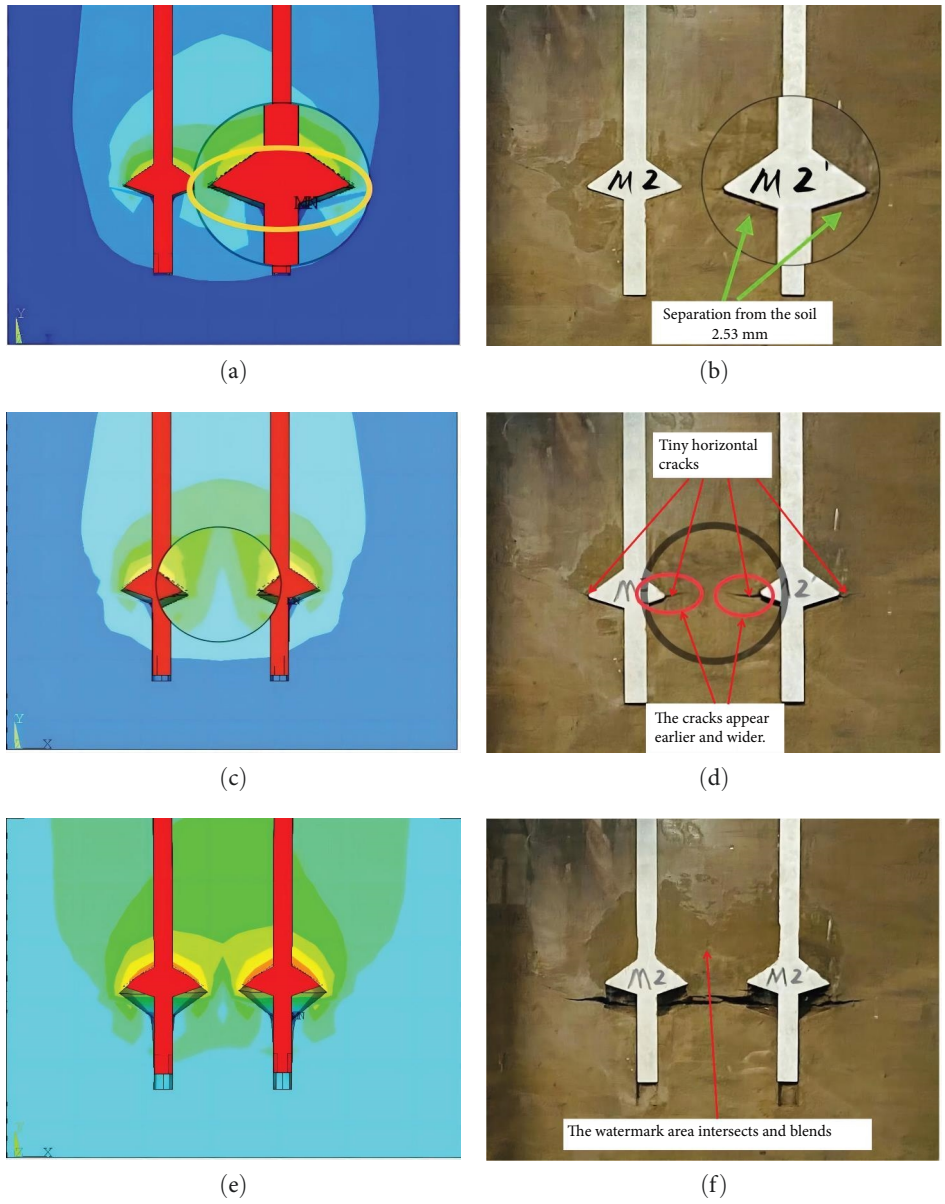

Figure 13: The final failure state comparison diagram of NT-CEP double piles (a)–(f).

(2) In the middle stage of loading, with a continuous increase in load, the soil on the plate is compressed and exhibits a noticeable displacement when the load reaches 3,200 kN, which indicates that the bearing plate began to function as intended at this point. However, owing to the small range of influence of the soil, the four piles still worked independently and did not affect each other, as shown in Figure 16(c). When the load increased from 3,200 to 5,600 kN, the overall displacement of the pile increased gradually, and the influence range of the soil on the pile expanded outward continuously until they connected with each other. In this process, the influence range of the soil involves only the soil between the piles and near the plate, as shown in Figure 16(d)–16(f). In the second half of this process, the compressed soil on each NT-CEP pile plate overlapped, and the four piles shifted from working independently to resisting the loads. However, the displacement of the soil between the piles is still small and has little effect on the bearing capacity of the foundation.

(3) At the later stage of loading, the affected area of soil on the plate presents an inverted "heart" distribution and first affects the central part of the four piles, as shown in Figure 16(g). Until the load reached 7,200 kN, the influence range diffused from the center to the external soil of the four piles, which shows that the damage to the soil around the piles when squeezed by the bearing plate was from the inside to the outside, as shown in Figure 16(h). At this stage,

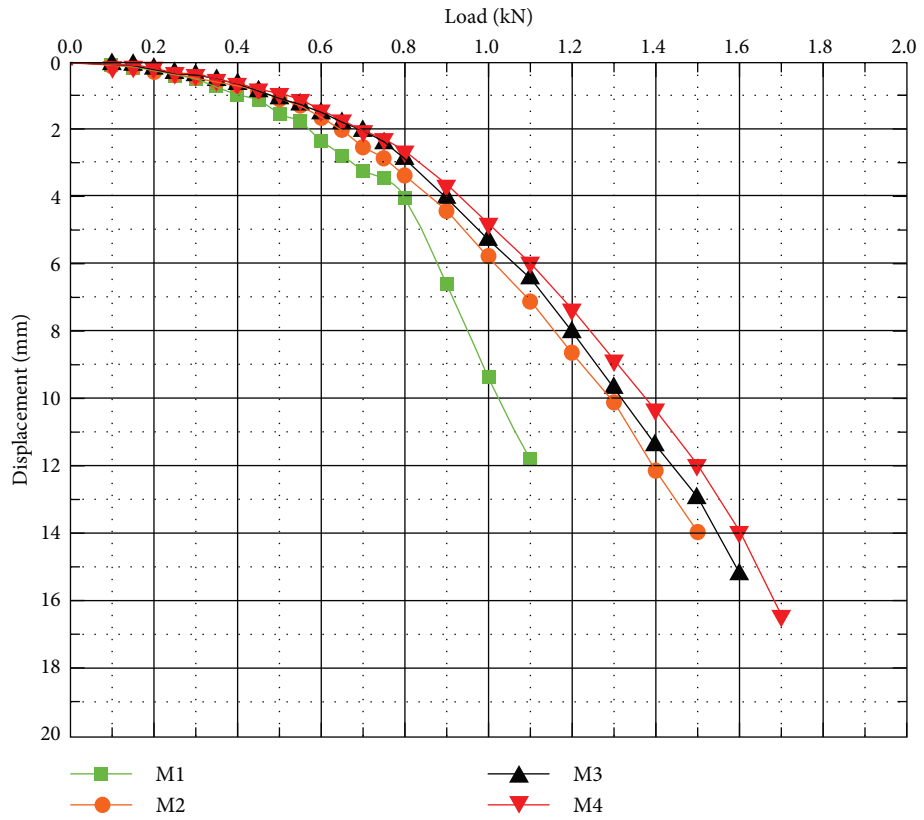

Figure 14: Load–displacement curve of the model test.

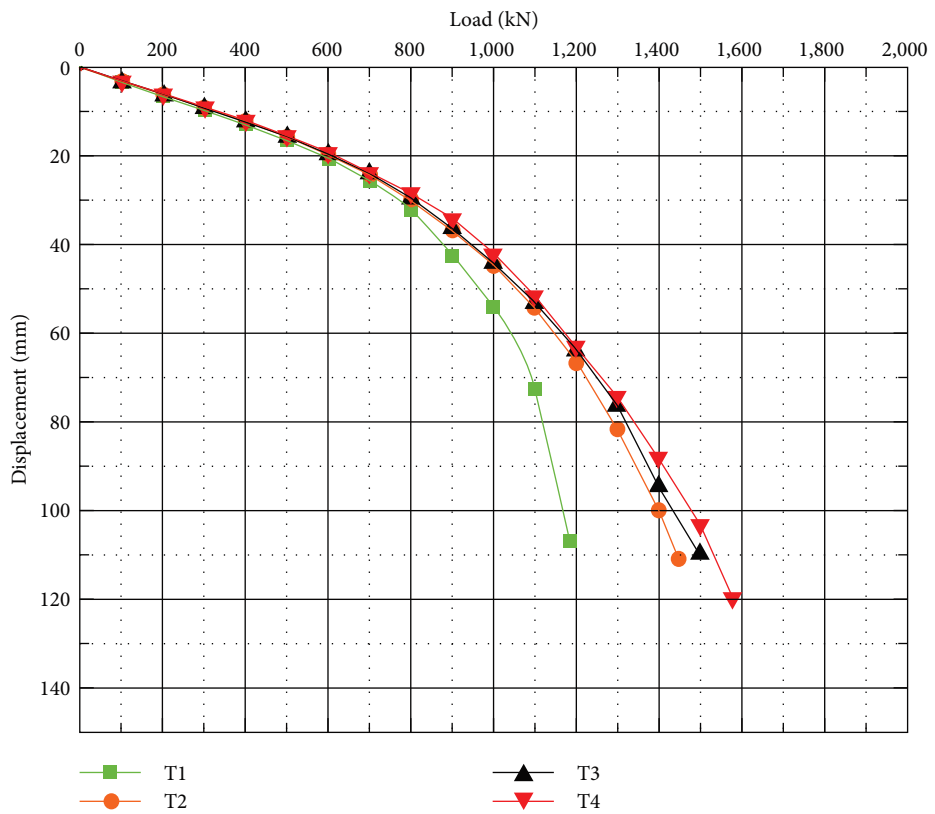

Figure 15: Simulation analysis of load–displacement curve.

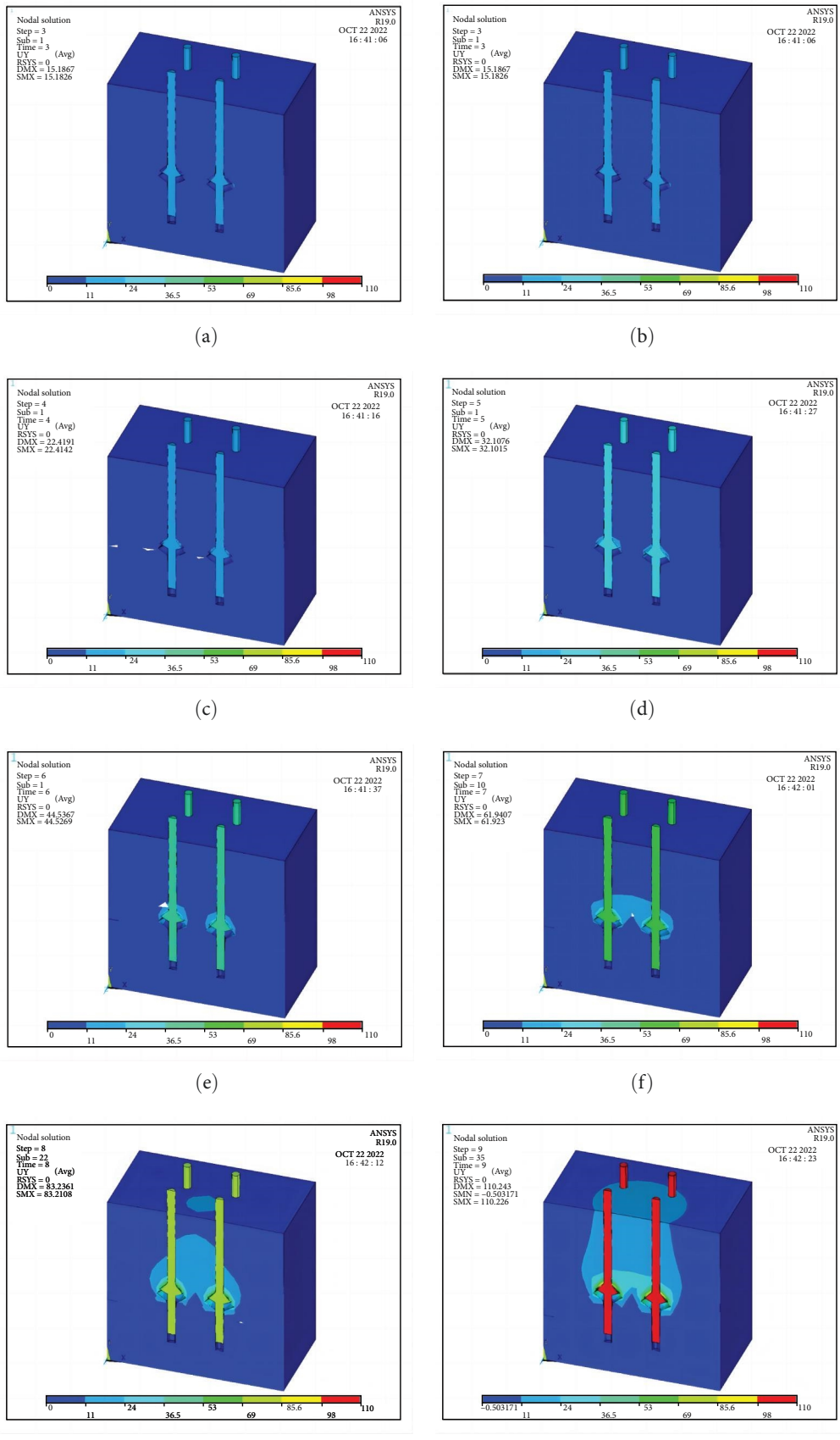

FIGURE 16: *Y*-direction displacement cloud diagram of the F6 group during loading: (a) 1,600 kN; (b) 2,400 kN; (c) 3,200 kN; (d) 4,000 kN; (e) 4,800 kN; (f) 5,600 kN; (g) 6,400 kN; (h) 7,200 kN.

the displacement of the pile top exceeds the limit displacement, and the ANSYS simulation analysis no longer converges.

7.2. Displacement Nephogram Analysis of Six Piles during the Loading Process. The displacement nephogram in the S6 group was extracted during the simulation analysis of the six-pile models to observe the displacement under different loads in detail. The *Y*-direction displacement nephograms were extracted under loads of 1,200, 2,400, 3,600, 4,800, 6,000, 7,200, 8,400, and 9,600 kN, respectively, as shown in Figure 17.

The following can be observed from the change in displacement nephogram in Figure 17:

(1) When the load was 1,200 kN, there was only one image color, and the displacement change in the pile relative to the soil was not noticeable. When the load reached 2,400 kN, the color of the six piles changed, and the displacement of the piles relative to the soil changed significantly, as shown in Figures 17(a) and 17(b). Similar to the loading process of the four-pile model, this process can be regarded as the initial stage of loading, and the NT-CEP piles in this stage rely on side friction to resist the loads.

(2) As the load increased to 3,600 kN, the color changed. Meanwhile, the soil was squeezed, and displacement occurred, as shown in Figure 17(c). As the load continued to increase, the displacement of the pile relative to the soil became more evident, and the compression range of the soil increased continuously until the load reached 6,000 kN. The influence ranges of the soil on the upper side of the load-bearing plate are connected with each other and located close to the middle pile and melt into each other, showing an "arch" phenomenon, as shown in Figures 17(d) and 17(e). At this point, the NT-CEP piles interacted with each other, and the soil exhibited an upward displacement. When the load reached 7,200 kN, the influence range of the soil continued to spread upward to the top surface of the soil following the "arch" characteristic, and the color change of the middle two piles is more evident than that of the piles on both sides. This indicates that the displacement of the two side piles in the middle was larger than that of the corner piles on both sides, and the soil in the middle was affected more. This process can be regarded as the middle stage of loading. At this stage, the NT-CEP piles exhibited clear interactions. Under the action of the load-bearing plates, the piles on both sides squeezed the middle soil and caused its entirety to experience a greater upward force, as shown in Figure 17(f).

(3) When the load reached 8,400 kN, the relative displacement of the pile body increased again, the range of influence of the soil on the upper side of the load-bearing plate was approximately cylindrical, and the color of the soil on the upper side near the load-bearing plate became darker. Meanwhile, the soil on the upper side of the load-bearing plate continued to be squeezed, and the overall effect of the six piles was more evident. However, when the load reached 9,600 kN, the color of the middle side pile and the corner pile deepened again, and the soil exhibited an "arch" upward trend again, indicating that the squeezed displacement of the upper side soil at this point increased once more, as shown in Figures 17(g) and 17(h). This process can be regarded as the later stage of loading, in which the displacement of the pile top approaches the ultimate displacement, and the corner pile gradually reaches the limit load after the middle pile reaches the limit load.

7.3. Displacement Nephogram Analysis of Nine Piles during the Loading Process. The displacement nephogram of the NT-CEP piles in the N6 group and the soil around the piles in the simulation analysis process of nine piles were extracted to observe the displacement under different loads in detail. The Y-direction displacement nephograms under loads of 1,800, 3,600, 5,400, 7,200, 9,000, 10,800, 12,600, and 14,400 kN were obtained, as shown in Figure 18.

The following can be observed from the change in displacement nephogram in Figure 18:

(1) At the initial stage of loading, when the load is 1,800 kN, the pile body of nine piles has an evident color change compared with the soil body, and the soil body near the bearing plate exhibited a noticeable color change, which indicates that the pile body was displaced and the bearing plate began working as intended. This differs from the phenomenon observed after the first stage loading of the four- and six-pile models because the number of piles in the N6 group is greater, the pile group effect is more noticeable, and the bearing capacity of each single pile decreases more. When the load was increased to 3,600 kN, the soil around the pile appeared to have a pear-shaped influence range starting from the bearing plate, which includes the soil on the plate as well as the soil under the plate, indicating that the nine piles of the NT-CEP pile had a strong overall action at this point, as shown in Figures 18(a) and 18(b).

(2) With the increase in load, the displacement of the pile body increased in the middle stage of the whole loading, and the influence range of the soil around the pile also continuously increased. When the load reached 10,800 kN, it can be observed that the influence range of the soil around the pile expanded to the boundary of the soil model, which further reflects the overall failure nature of the nine-pile model, as shown in Figure 18(c)–18(f).

(3) When the load was 12,600 kN, the soil around the pile was compressed again, resulting in secondary

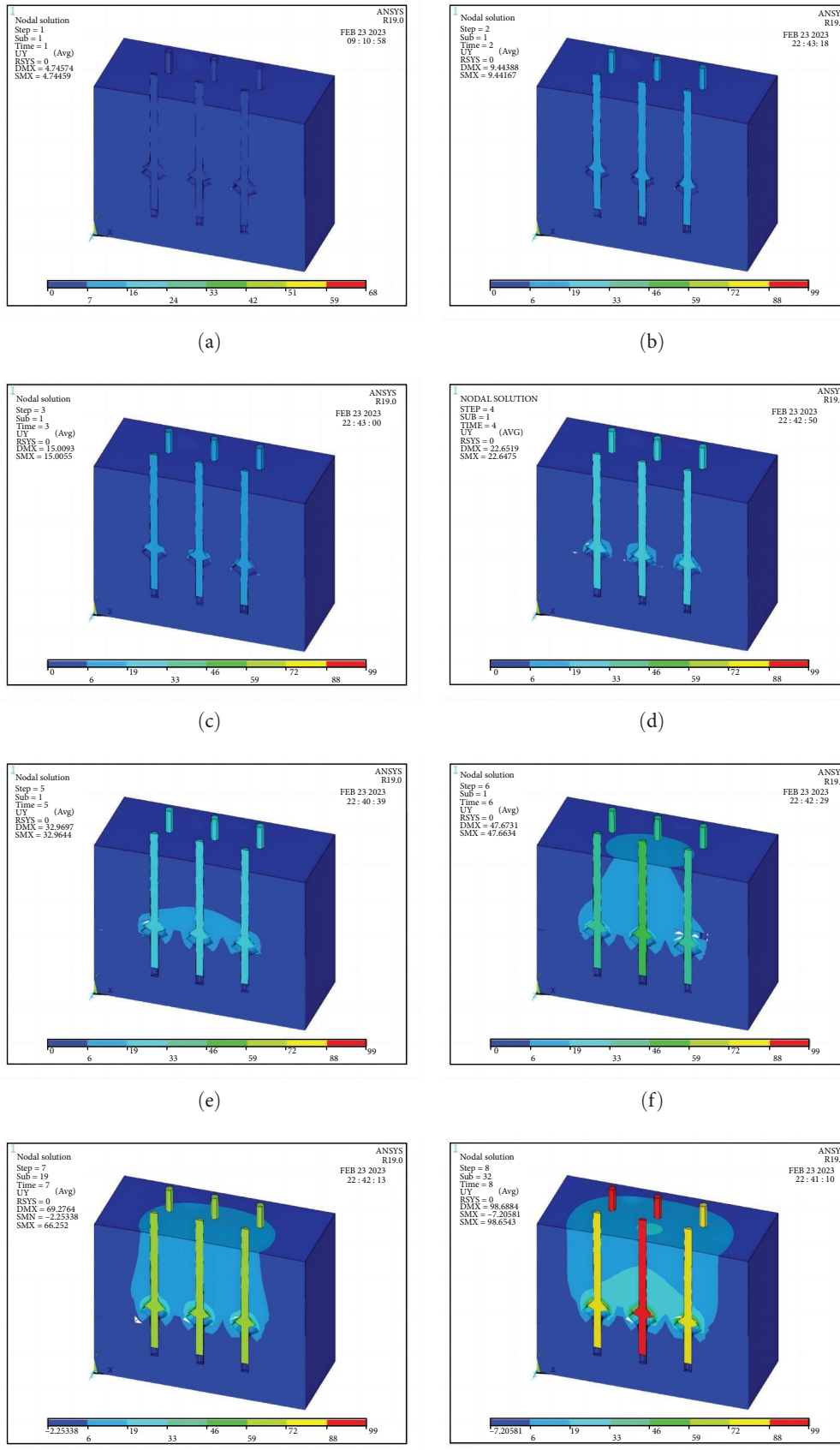

FIGURE 17: *Y*-direction displacement nephogram of S6 group loading: (a) 1,200 kN; (b) 2,400 kN; (c) 3,600 kN; (d) 4,800 kN; (e) 6,000 kN; (f) 7,200 kN; (g) 8,400 kN; (h) 9,600 kN.

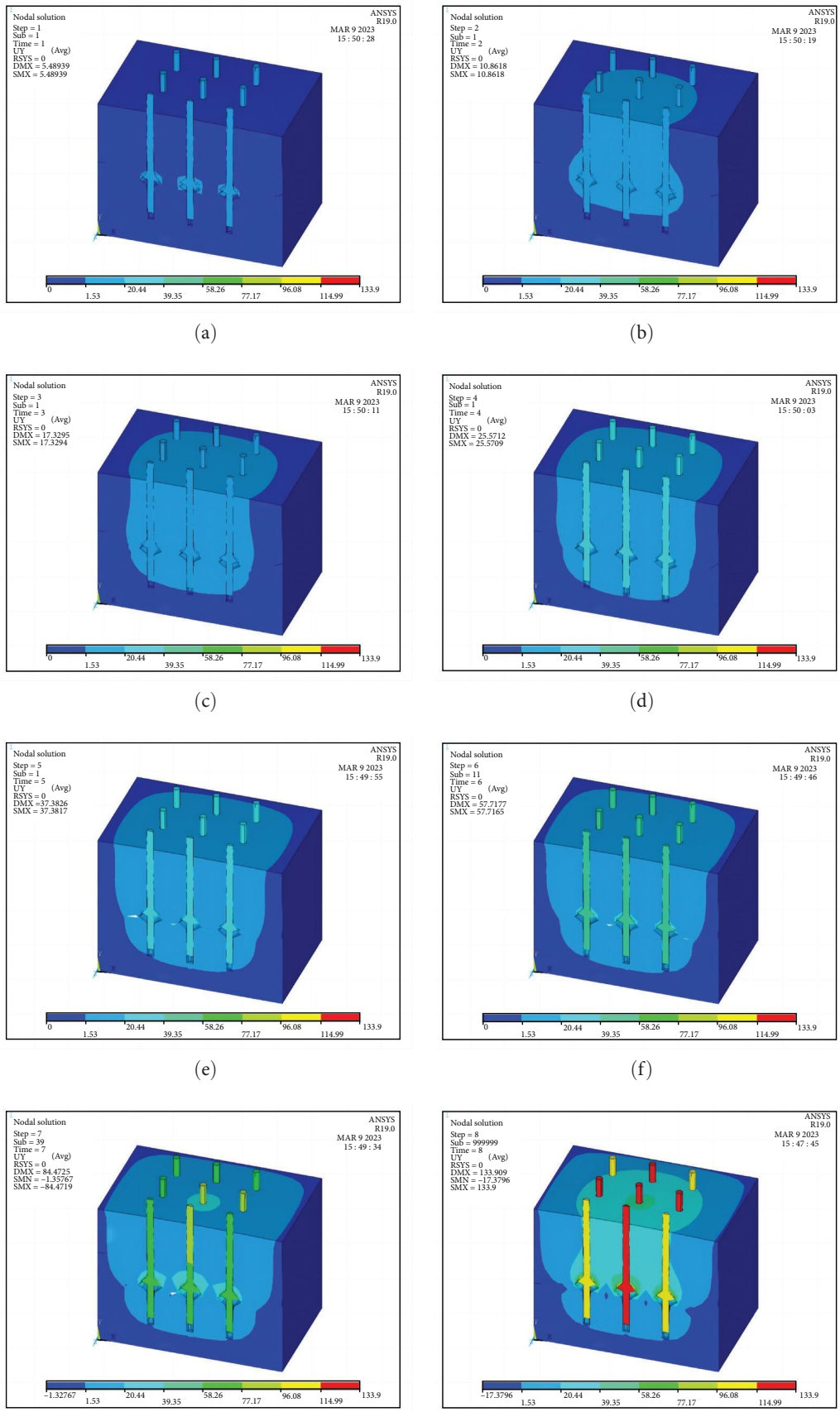

FIGURE 18: *Y*-direction displacement nephogram of the N6 group loading: (a) 1,800 kN; (b) 3,600 kN; (c) 5,400 kN; (d) 7,200 kN; (e) 9,000 kN; (f) 10,800 kN; (g) 12,600 kN; (h) 14,400 kN.

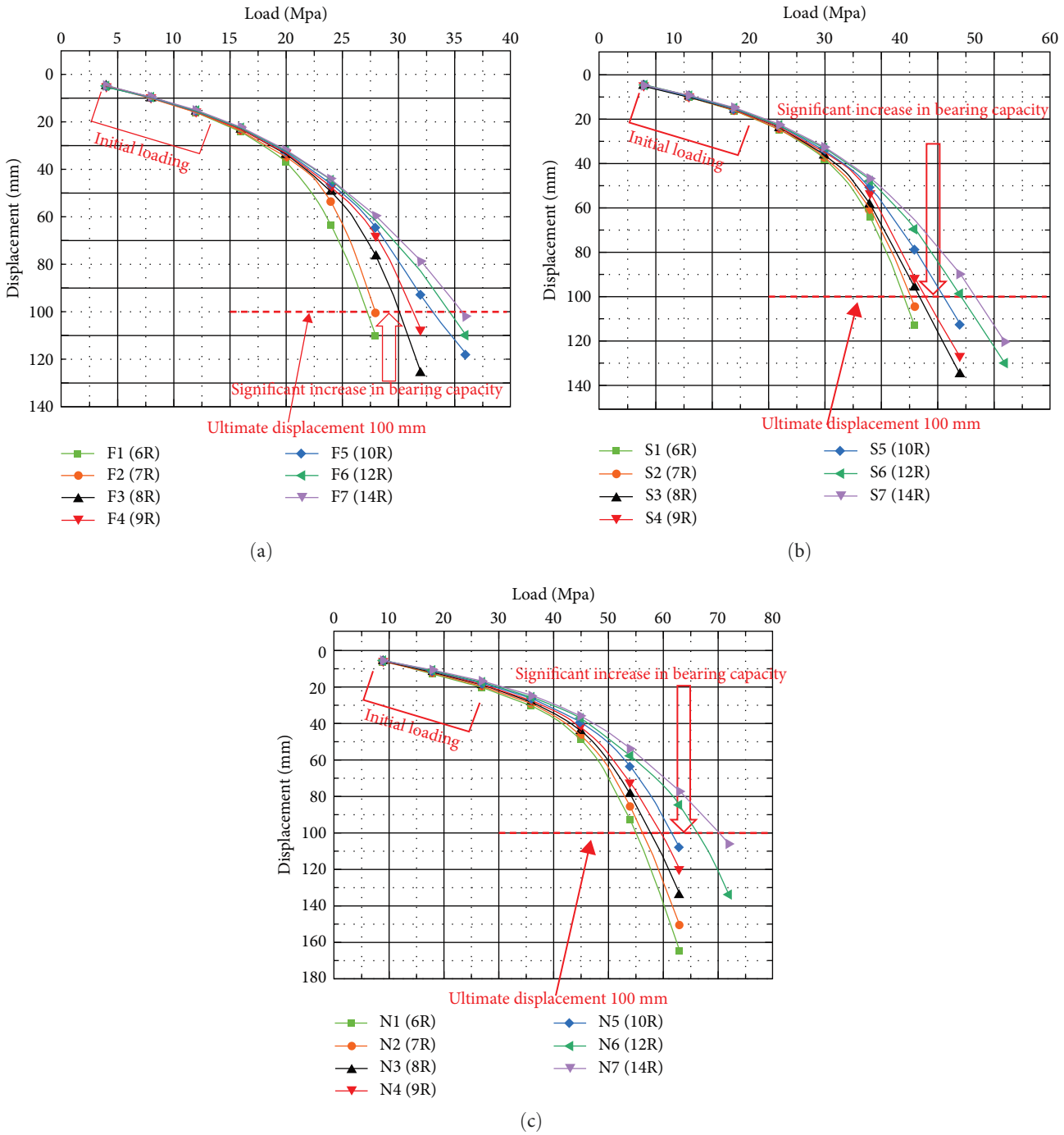

Figure 19: Load–displacement curve: (a) load–displacement curve of four-pile models; (b) load–displacement curve of six-pile models; (c) load–displacement curve of nine-pile models.

displacement, which was the most significant near the bearing plate. The soil surface near the central pile also exhibited obvious displacement, indicating that the central pile was affected by side and corner piles at this time, resulting in more serious damage to the soil around the central pile, and the pile group effect was more obvious. When the load reached 14,400 kN, the displacement of the pile body

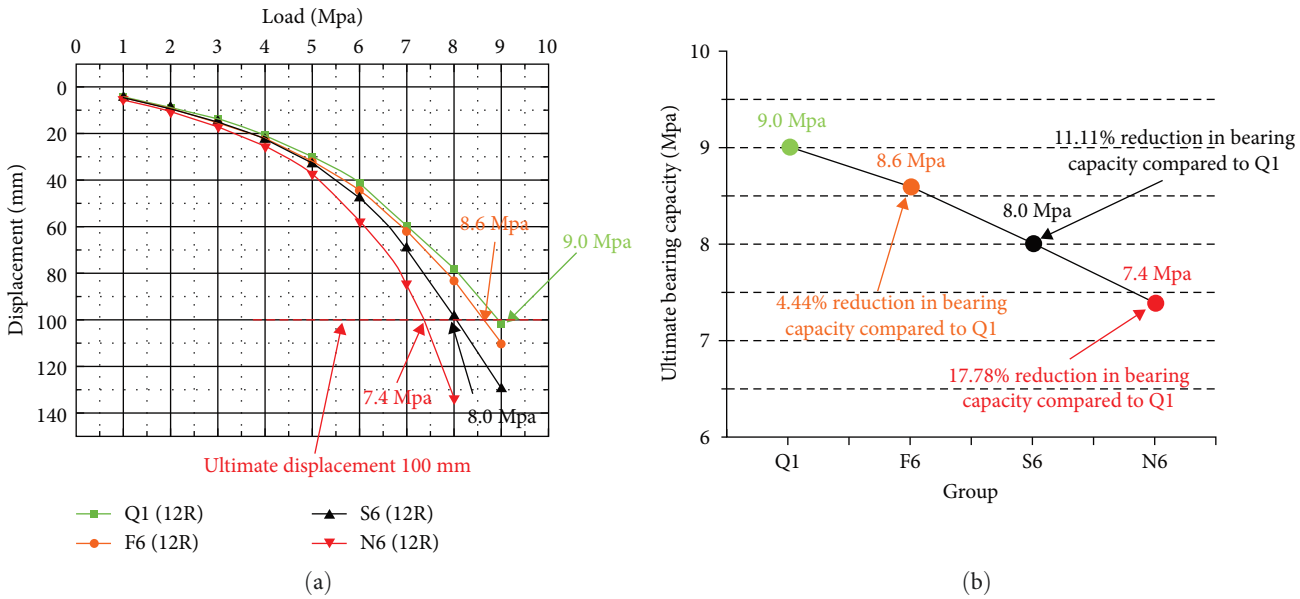

Figure 20: Comparison diagram between single piles and single piles in the pile group: (a) load–displacement curves of single piles and single piles in the pile group; (b) ultimate bearing capacity curves of single piles and single piles in the pile group.

continued to increase, the second displacement range of the soil around the pile expanded outside the range of nine piles again, the displacement of the center pile, side pile, and corner pile also increased again, and the order of failure followed the order center pile–side pile–corner pile, as shown in Figures 18(g) and 18(h).

8. Comparative Analysis of Load–Displacement Curves of the Pile Groups

Analyzing the load–displacement curve of Figure 19 shows that:

(1) The changing trend of the load–displacement curve of each group of piles at the initial stage of loading is typically the same; that is, with an increase in the load, the vertical displacement of the pile top also increases continuously, showing an almost linear change trend. Meanwhile, the pile top displacements of the three groups of model piles, Figure 19(a)–19(c), were all small. The NT-CEP piles in this stage relied on side friction to resist the load. As the load continued to increase, the pile-side friction was insufficient to bear all the vertical loads, and the load-bearing plates participated in the work. Because of the different positions of the load-bearing plates in each group, the load–displacement curves exhibit different trends.

(2) By comparing and analyzing each group of curves, results showed that each group of curves has a section where the ultimate bearing capacity increases rapidly. Figure 19(a) is between F2 and F3; Figure 19(b) is between S4 and S5, and Figure 19(c) is between N5 and N6. This indicates that when designing uplift piles, the position of the bearing plate (the distance from the top of the bearing plate to the top of the pile) should be larger than 7R when four piles are arranged ($R = 800$ mm is the overhang diameter of the plate), 9R when six piles are arranged, and 10R when nine piles are arranged, which can effectively improve the bearing capacity of the piles.

(3) Observing the load–displacement curves of each group, the displacement under the same load was $14R < 12R < 10R < 9R < 8R < 7R < 6R$ in the middle and later periods of loading. Therefore, whether it is a four-, six-, or nine-pile model, the lower the plate position, the better the bearing capacity of the NT-CEP pile.

9. Comparative Analysis of Curves of Single Pile and Single Pile in Pile Group

The single piles in F6, S6, and N6 in Figure 20 select the single pile with the largest displacement in the pile group, which are the corner, side, and middle piles in four, six, and nine piles, respectively.

From the load–displacement curves of a single pile and a single pile in the pile group in Figure 20(a), it can be observed that when the pile top load is considerably small, the four groups of curves almost coincide, which shows that the single piles in the pile group do not interact with each other and the pile group effect is not reflected. When the pile top load exceeds 2 MPa, the curves exhibit different trends, indicating that under the same load, the greater the number of piles, the greater the displacement and the lower the bearing capacity. Furthermore, the pile-group effect gradually increased. This trend continued up to the displacement limit. The bearing capacity of a single pile followed the order $Q1 > F6 > S6 > N6$.

From the ultimate bearing capacity curve of a single pile and single piles in the pile group in Figure 20(b), it can be seen that the bearing capacity of single, four, six, and nine piles are 9.0, 8.6, 8.0, and 7.4 MPa, respectively, which are reduced by 4.44%, 11.11%, and 17.87%, respectively, compared with Q1. The pile-group effect is evident and should be considered in the design calculations.

10. Conclusion

Through the experimental study and finite element simulation analysis of the NT-CEP pile group model with different disk positions, the following conclusions are drawn:

(1) The failure range of the soil around the NT-CEP pile group was not a simple addition of several individual piles. Because of the mutual influence between the piles, the failure range of the soil coincides, and the soil in the overlapping range exhibits aggravated failure. With an increase in the number of piles, the failure range of the soil in the two-, four-, six-, and nine-pile models also increased, and the pile-group effect was stronger.

(2) The displacement of a single pile at different positions in the NT-CEP pile group model follows the order middle pile > side pile > corner pile.

(3) With an increase in the number of piles (two-, four-, six-, and nine-pile models), the sum of the bearing capacities of the pile groups increased. However, owing to the effect of the pile group, the bearing capacity of a single pile in the pile group decreased continuously, and the greater the number of piles, the greater the decrease, which should be considered in the design calculation.

(4) In the same number of NT-CEP pile groups, $L1$ (the distance from the top of the load-bearing plate to the top of the pile) was greater than 4R. When $L1$ was greater than 4R, the lower the load-bearing plate was, the higher the overall bearing capacity of NT-CEP pile groups was.

(5) $L1$ (the distance from the top of the bearing plate to the top of the pile) should be greater than 7R ($R =$ 800 mm is the overhang diameter of the plate) when four piles are arranged, 9R when six piles are arranged, and 10R when nine piles are arranged. This can effectively improve the bearing capacity of NT-CEP piles.

Therefore, in the uplift design of the NT-CEP pile groups, the load-bearing expansion plate should be preferentially arranged at the lower part of the pile body when the soil parameters allow. When the soil condition is poor, the bearing plate should be close to the corresponding key position as far as possible to efficiently improve the bearing capacity of the NT-CEP pile. When the design is partial to safety, the design of the middle pile, side pile, and corner pile should take the bearing capacity of the middle pile as the design benchmark.

Data Availability

The data used to support the findings of this study are available from the corresponding authors upon request.

Conflicts of Interest

The authors declare that they have no known competing financial interests or personal relationships that could have appeared to influence the work reported in this paper.

Acknowledgments

This work was financially supported by the Jilin Provincial Science and Technology Department Excellent Talent Team Project (no. 20210509042RQ).

References

[1] X.-J. Gao, J.-C. Wang, and X.-R. Zhu, "Static load test and load transfer mechanism study of squeezed branch and plate pile in collapsible loess foundation," *Journal of Zhejiang University-SCIENCE A*, vol. 8, no. 7, pp. 1110–1117, 2007.

[2] M. Zhang, P. Xu, W. Cui, and Y. Gao, "Bearing behavior and failure mechanism of squeezed branch piles," *Journal of Rock Mechanics and Geotechnical Engineering*, vol. 10, no. 5, pp. 935–946, 2018.

[3] H.-W. Ma, Y.-Y. Wu, Y. Tong, and X.-Q. Jiang, "Research on bearing theory of squeezed branch pile," *Advances in Civil Engineering*, vol. 2020, Article ID 6637261, 12 pages, 2020.

[4] Y. Ju and Y. F. Chen, "Experimental study for the bearing capacity calculation of concrete expanded plates in squeezed branch piles," *Materials Testing*, vol. 60, no. 11, pp. 1118–1124, 2018.

[5] Y. Wang, X. Feng, and M. Zhang, "Experimental study on the bearing characteristics of squeezed branch piles," *Journal of Henan Polytechnic University (Natural Science)*, vol. 33, no. 6, pp. 799–803, 2014.

[6] T. Li, P. Xu, and G. Yang, "Investigation into bearing performance of concrete expanded-plates piles: field test and numerical modelling," *Engineering Structures*, vol. 271, Article ID 114954, 2022.

[7] L. Xiong, G. Li, Y. Zhou, and G. He, "Experimental and analytical investigation of the bearing capacity of bulbs for squeezed branch piles," *International Journal of Geomechanics*, vol. 23, no. 5, 2023.

[8] D. A. Brown, C. Morrison, and L. C. Reese, "Lateral load behavior of pile group in sand," *Journal of Geotechnical Engineering*, vol. 114, no. 11, pp. 1261–1276, 1988.

[9] S. T. Tang and L. H. Chen, *Field test of DX pile group[C]// Advanced Materials Research*, vol. 243, pp. 2451–2455, Trans Tech Publications Ltd., 2011.

[10] D. H. Hadi, M. Q. Waheed, and M. Y. Fattah, "Effect of pile's number on the behavior of piled raft foundation," *Engineering and Technology Journal*, vol. 39, no. 7, pp. 1080–1091, 2021.

[11] M. Y. Fattah, M. A. Al-Obaydi, and F. A. Al-Jalabi, "Effect of number of piles on load sharing in piled raft foundation system in saturated gypseous soil," *International Journal of Civil Engineering and Technology (IJCIET)*, vol. 9, no. 3, pp. 932–944, 2018.

[12] A. S. Al-Suhaily, A. S. Abood, and M. Y. Fattah, "Bearing capacity of uplift piles with end gates," in *Proceedings of*

China-Europe Conference on Geotechnical Engineering, vol. 2, pp. 893–897, Springer International Publishing, 2018.

[13] P. Cheng, Y. Liu, Y. P. Li, and J. T. Yi, "A large deformation finite element analysis of uplift behaviour for helical anchor in spatially variable clay," *Computers and Geotechnics*, vol. 141, Article ID 104542, 2022.

[14] P. Cheng, F. Liu, X. Chen, Y. Zhang, and K. Yao, "Estimation of the installation torque-capacity correlation of helical pile considering spatially variable clays," *Canadian Geotechnical Journal*, 2024.

[15] P. Cheng, J. Guo, K. Yao, and X. Chen, "Numerical investigation on pullout capacity of helical piles under combined loading in spatially random clay," *Marine Georesources & Geotechnology*, vol. 41, no. 10, pp. 1118–1131, 2023.

[16] X.-J. Chen, Y. Fu, and Y. Liu, "Random finite element analysis on uplift bearing capacity and failure mechanisms of square plate anchors in spatially variable clay," *Engineering Geology*, vol. 304, 2022.

[17] Y. H. Li, X. J. Gao, and G. H. Zhong, *Model Test and Finite Element Analysis of Squeezed and Branch Pile bBared Vertical and Horizontal Loads[C]//Applied Mechanics and Materials*, vol. 470, pp. 1101–1104, Trans Tech Publications Ltd., 2014.

[18] K. C. Onyelowe, A. M. Ebid, E. Ramani Sujatha et al., "Extensive overview of soil constitutive relations and applications for geotechnical engineering problems," *Heliyon*, vol. 9, no. 3, Article ID e14465, 2023.

[19] K. Zeng, D. Pal, H. J. Gong, N. Patil, and B. Stucker, "Comparison of 3DSIM thermal modelling of selective laser melting using new dynamic meshing method to ANSYS," *Materials Science and Technology*, vol. 31, no. 8, pp. 945–956, 2015.

[20] L. Tao, Z. Jie, and X. Long, "The influence of modeling methods on the meshing when solid element was used in ANSYS—taking the design by analysis of dry welding experiment module as an example," *Applied Mechanics and Materials*, vol. 42, 2010.